^{3}He specific heat and thermometry at millikelvin temperatures

Dennis S. Greywall
AT&T Bell Laboratories, Murray Hill, New Jersey 07974
(Received 24 September 1985)

High-precision specific-heat measurements were made on pure liquid ^{3}He in both the normal and superfluid phases for temperatures between 0.6 and 5 mK and for pressures between 0 and 34 bars. The data were obtained using a magnetic susceptibility thermometer which was calibrated against the National Bureau of Standards scale near 15 mK and at lower temperatures principally by the condition that the zero-pressure normal-phase specific heat be linear in temperature. The ^{3}He phase diagram based on this scale is presented. In particular we find that $T_A = 2.49$ mK which differs quite substantially from the currently accepted value of about 2.7 mK. Multiplying the Pt NMR temperatures determined by Haavasoja and co-workers by a factor of 0.89 or subtracting 0.13 mK from the magnetic temperatures of Paulson *et al.* brings both of these scales into excellent agreement with the new scale. The ^{3}He quasiparticle effective mass, $m_3^*(P)$, extracted from the normal-phase data agrees well with our previously reported results based on higher-temperature specific-heat data. The values of $m_3^*(P)$ from Haavasoja and co-workers are $\sim 20\%$ smaller. However, if their specific-heat data are reanalyzed using the new temperature scale, the two sets of $m_3^*(P)$ values are brought into good agreement. We thus claim that the large discrepancies between previous specific-heat measurements are due almost entirely to differences in temperature scales. The new normal-phase specific-heat data at low pressures show no evidence of the anomalous behavior observed by Haavasoja and co-workers. Consequently, the size of the specific-heat jump at T_c could be determined with little ambiguity over the entire pressure range. $\Delta C/C_>$ is only a few percent larger than the weak-coupling value at $P=0$ and increases linearly with sample density. At high density the temperature dependence of the specific heat below T_c shows small deviations from theory.

I. INTRODUCTION

Two recent low-temperature experiments,[1,2] designed primarily to study the specific heat of superfluid ^{3}He, yielded remarkably similar results. However, the data for the normal-phase specific heat were much smaller than and clearly inconsistent with earlier measurements[3–7] made generally at somewhat higher temperatures. The large discrepancy could not be explained beyond conjecture, and consequently it was not known which of the two groups of experiments was giving the correct ^{3}He specific heat and therefore the correct ^{3}He quasiparticle effective mass m_3^*.

More recently, additional specific-heat measurements[8] were made on the normal phase of the liquid. These precise data covered large ranges of both temperature and pressure, and fell between the extremes of the previous results, but much closer to the older higher-temperature data. It was demonstrated that only this newest set of measurements satisfied several important thermodynamic checks. Support for these data was also provided by two subsequent normal-phase specific-heat experiments[9,10] performed, however, only over limited ranges of temperature and pressure. Moreover, it has been demonstrated[11] that the newest determination of m_3^* is the most compatible with our current theoretical understanding of liquid ^{3}He.

Obviously, if the newest values[8] of m_3^* are accepted as correct, then the recent very-low-temperature specific-heat data[1,2] on ^{3}He, including the results for the superfluid phases, must be seriously in error. One must thus question, for example, the reliability of the deviations from BCS theory extracted from these measurements. Furthermore, since the source of error is unknown one cannot be certain that the problem is confined solely to the specific heat of ^{3}He.

In this paper we present new high-precision specific-heat results for liquid ^{3}He which cover the temperature range 0.6—5 mK and the pressure range 0—34 bars. The data were obtained using a magnetic-susceptibility thermometer which was calibrated against the National Bureau of Standards (NBS) temperature scale[12] (CTS-1983) near 15 mK and at lower temperatures principally by the condition that the zero-pressure normal-phase specific heat be linear in temperature. C/T was found to be in good agreement with values from Ref. 8. It was also found that the new temperature scale is accurately proportional to the platinum NMR scale of Ref. 1 with a scaling factor of 0.89. On the new scale the superfluid transition temperature at melting pressure is 2.49 mK. If the specific-heat data of Refs. 1 and 2 are reanalyzed using the new temperature scale, their normal-phase values are brought into very good agreement with the specific-heat data presented in this paper and with the results of Ref. 8. We therefore find the source of the ^{3}He specific-heat controversy to be entirely associated with differences in thermometry.

The new low-pressure specific-heat data near the superfluid transition (at T_c) do not show any evidence of the anomalies seen by Ref. 1 in the normal phase and by Ref.

2 in the superfluid phase. Consequently the size of the specific-heat jump at T_c could be determined with little ambiguity over the entire pressure range. $\Delta C/C_>$ is only a few percent larger than the weak-coupling value at $P=0$ and increases linearly with sample density. At high density the temperature dependence of the specific heat below T_c shows small deviations from theory.[13]

II. EXPERIMENTAL DETAILS

A. Calorimeter

Figure 1 shows a cross-sectional drawing of the calorimeter and also the attachment of the sample cell to the $PrNi_5$ refrigerator. Some technical details of the calorimeter are listed in Table I. Specifics of the nuclear demagnetization refrigerator are discussed in Ref. 14. The cell had a nominal volume of 17 cm^3 and was constructed mainly from high-purity silver because of this material's small nuclear specific heat.

Located inside the cell and soldered[15] to its base were six 3-mm-diam silver rods. These extended to near the top of the cell. Silver powder[16] was sintered[17] around each of these rods using a graphite mold to form posts 0.9 cm in diameter and 0.9 cm high. The Brunauer-Emmett-Teller (BET) surface area measured before sealing[18] the cover onto the cell base was 9.3 m^2. This corresponds to 0.83 m^2 per gram of silver powder, which agrees well with previous[19] measurements made on small-diameter plugs sintered under similar conditions. The calorimeter heater was noninductively wound around one of the silver posts just above the sintered material. It consisted of a 7.6-cm length of 0.0025-cm-diam Pt-W wire with a resistance of 116 Ω. The heater leads were 0.0076-cm-diam Cu-Ni–clad Nb-Ti wires. The lanthanum-diluted cerium magnesium nitrate thermometer (see Sec. II B) was located inside a high-purity[20] niobium shield which threaded into

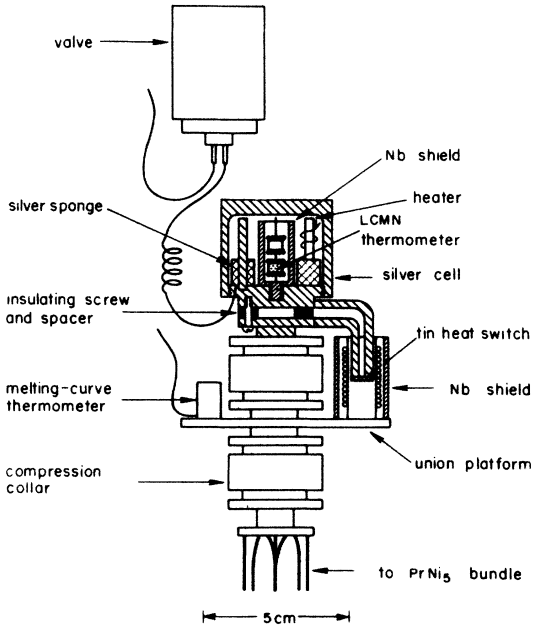

FIG. 1. Calorimeter.

TABLE I. Calorimeter details.

Sample volume	16.55 cm^3
Volume of silver sinter	2.7 cm^3
Surface area of sinter	9.3 m^2
Heater resistance	116.3 Ω
Principal construction materials	
Silver	238.5 g
Silver powder	11.2 g
Niobium	5.45 g
Copper	0.7 g
Pt-W	0.002 g

the cell base. Six 1-mm-diam holes were drilled through the shield very near the closed bottom of the cylinder to admit the ^{3}He sample when the calorimeter was only partially full. The electrical leads to the heater and to the thermometer passed out of the ^{3}He chamber through short lengths of copper capillary tubing epoxied[18] into holes drilled through the cell base. The seals between the wires and the tubing were also made with epoxy.[21]

The cell was positioned above a flanged silver post which was, in turn, mechanically clamped[22] to the nuclear refrigerator. Rigid support was provided by three pairs of thermally insulating Vespel[23] screws and spacers. Contact was also made via two pairs of 3-mm-diam silver rods which were welded to the cell base and flange, respectively, and joined at their opposite ends with a tin heat switch. This switch was activated using a superconducting coil attached to the union platform of the refrigeration, see Fig. 1. To confine the magnetic field, the coil was located inside a Nb shield. A 0.1-Ω shunt across the leads of the coil was thermally attached to the still of the dilution refrigerator.

In addition to the heat-switch coil, a melting-curve (MC) thermometer,[24] a 20-pF reference capacitor,[14] and a pressure gauge were mounted on the union platform. The pressure gauge was identical in construction to the MC thermometer and was joined to the cell with a 6-cm length of 0.0076-cm-i.d. Cu-Ni capillary. The fill capillary was similar but had a length of ~1 m between the cell and the valve[25] mounted on the mixing chamber of the dilution refrigerator. To prevent the coiled capillary from vibrating it was wound in the threads of a nylon screw which was attached to one of the support rods of the nuclear refrigerator.

B. Thermometry

The cell temperature was measured using a LCMN thermometer located inside the cell (Fig. 1) and in direct contact with the ^{3}He sample. The low-temperature part of the thermometer consisted of a pair of superconducting coils[24] which formed two legs of a self-inductance susceptibility bridge[26] operated at a frequency of 1 kHz. The coils were made as identical as possible, except that one coil was firmly packed with finely powdered LCMN (5 at. % CMN) forming a plug 4.8 mm in diameter and 4.8

mm in height. The plug was covered at both ends by discs of coarse filter paper. The two coils were epoxied into holes drilled into a sheet of plastic. In turn, the strip of plastic was inserted into a niobium tube which was rigidly attached to the cell body. To reduce the trapped magnetic field in the niobium cylinder, a μ-metal shield was placed around the outside of the Dewar during the initial cooldown of the cryostat.

The resolution of the thermometer was given approximately by

$$\frac{\delta T}{T} \approx 1.6\times 10^{-4}\frac{T}{V} .$$

T is the temperature measured in mK, and V is the rms bridge excitation voltage in mV. The self-heating in the thermometer was described by

$$\frac{\Delta T}{T} \approx 3.0\times 10^{-5}\frac{V^2}{T} .$$

The heat-capacity measurements were made with the bridge driven at 1 mV for $T<1.5$ mK and at 2 mV for higher temperatures. Therefore the self-heating at 0.7, 1.5^-, 1.5^+, and 5 mK was 4×10^{-5}, 2×10^{-5}, 8×10^{-5}, and 2×10^{-5}, while the corresponding resolution was 1×10^{-4}, 2×10^{-4}, 1×10^{-4}, and 4×10^{-4}. Consequently, in order that the heat-capacity data have a precision of better than 1%, it was necessary to generate temperature steps which were greater than 2%, 4%, 2%, and 8% of the temperature, respectively.

The preliminary calibration of the LCMN thermometer was performed by closing the cell heat switch and comparing the LCMN-thermometer readings with those of the MC thermometer mounted on the union platform (Fig. 1). This was done for various temperatures in the range 1–16 mK. A check on the accuracy of this mapping was made by comparing the superfluid transition line [i.e., $T_c(P)$] determined using the LCMN thermometer with that previously reported and based on the same melting-curve scale.[14] In particular, and in agreement with the previous work, it was found that $T_c(P=0)$ and T_S, the magnetic-ordering transition temperature, were numerically equal to within better than $\frac{1}{2}$%. The conclusion is that there were no serious temperature gradients between the LCMN and MC thermometers even though the thermal path included the tin heat switch and two rather-low-surface-area ^{3}He–to–silver-powder interfaces. The same conclusion was also reached based on a measurement of the small heat leak ($\sim$0.1 nW) into the cell.

The calibration data were well fitted by the expression

$$\frac{1}{T-\Delta} = A\left[\frac{R}{1-R}\right]+B , \qquad (1)$$

with Δ, A, and B as adjustable parameters. R is the bridge ratio and $R/(1-R)$ is proportional to the susceptibility. However, as will be discussed in detail in Sec. III, C/T for normal ^{3}He based on this calibration decreases with decreasing temperature, which is contrary to theoretical expectations and also to previous ^{3}He specific-heat experiments. We interpret this finding as an indication that the MC temperature scale[14] is giving temperatures which are too high in the millikelvin region. Note that the MC scale of Ref. 14 is based on the thermodynamic measurements of Halperin *et al.*[3] below $\sim$15 mK. We have therefore elected to adjust the temperature scale to give the expected temperature independence of C/T for normal ^{3}He at vapor pressure. That is, we use the normal-phase specific heat as an input in determining the working temperature scale which we then use primarily to analyze the measurements in the superfluid phases. The details of the temperature-scale adjustment are deferred to Sec. III because of their intimate connection with the final specific-heat results.

C. Specific-heat measurements

The heat-capacity measurements were made using the standard heat-pulse technique with both the heater and thermometer located inside the ^{3}He chamber. In contrast to other recent very-low-temperature specific-heat experiments[1,2] in which nominally 1-Ω pure copper or silver wire heaters were used, we employed a Pt-W heater element with a resistance of 116 Ω, the advantage of the alloy being that the resistance is nearly independent of wire temperature. The resistance was measured using a four-wire technique.

Figure 2 shows a typical specific-heat measurement. This point was taken in the superfluid phase with the cell filled at vapor pressure and at a temperature of 0.8 mK. The drift rate corresponds to a parasitic heat leak of $\sim$0.1 nW. Normally, data points were taken at intervals of roughly 10 min, which corresponds to more than 10 thermal time constants. Each ^{3}He sample was confined to constant volume using the valve mounted on the mixing chamber of the dilution refrigerator. The valve also eliminated time-dependent heat leaks into the calorimeter associated with ^{3}He flowing in or out of the cell due to temperature changes in the warmer parts of the cryostat.

Several sets of heat-capacity measurements were made at vapor pressure corresponding to different partial fil-

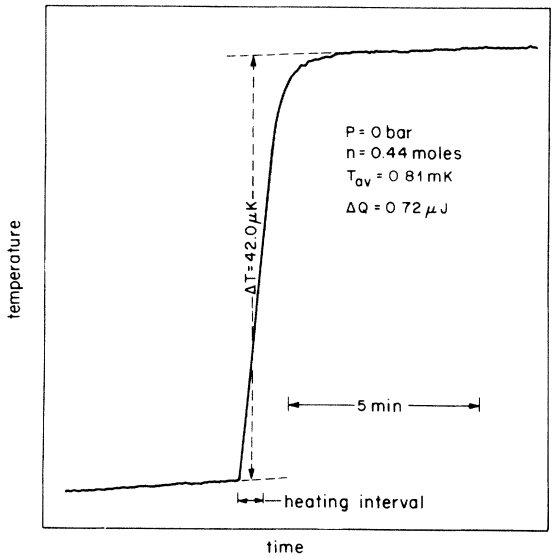

FIG. 2. Typical heat-capacity measurement.

lings of the cell. Each filling, however, was sufficient to completely cover the sintered-silver heat exchanger, see Fig. 1. The number of moles of ^{3}He admitted to the calorimeter was accurately measured using a calibrated 0.5-l volume located at room temperature.

Figure 3 shows the heat capacity measured at 5 mK plotted as a function of the number of moles of ^{3}He. The straight line drawn through the data points has a nonzero x-axis intercept. This means that a total of 0.0085 moles of ^{3}He (0.31 cm^3) are lost to the cold valve, to the pressure gauge on the union platform, and to the joining length of capillary tubing. This number is reasonable and consistent with the known volumes of the appendages. In this analysis the tacit assumption is that above a few millikelvin all background contributions to the heat capacity, including any possible surface contributions, are completely negligible.

For pressures greater than zero, the number of moles of sample was determined using a measurement of the cell volume and the zero-temperature molar-volume—versus—pressure data compiled by Wheatley.[27] These data are fitted by the expression

$$V=\sum_{i=0}^{5} a_i P^i , \tag{2}$$

with

$$a_0=36.837\,231,\quad a_1=-0.118\,034\,74\times 10^{1} ,$$

$$a_2=0.834\,214\,17\times 10^{-1},\quad a_3=-0.388\,595\,62\times 10^{-2} ,$$

$$a_4=0.947\,597\,80\times 10^{-4},\quad a_5=-0.912\,535\,77\times 10^{-6} .$$

V and P are in cm^3/mole and bars, respectively.

The low-temperature cell volume was determined by very slowly metering in ^{3}He and by detecting the point at which the cell was filled by the sharp increase in the cell pressure measured using the *in situ* gauge. The correction was then applied for the lost volume. It is estimated that the uncertainty in the cell-volume determination is $\frac{1}{2}\%$.

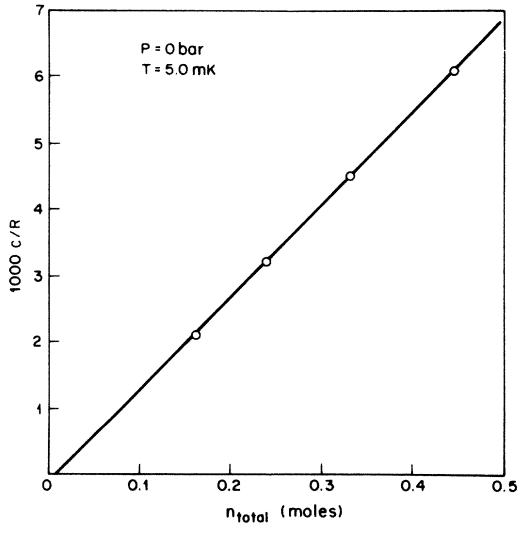

FIG. 3. Heat capacity measured at 5 mK versus the number of moles of ^{3}He admitted to the calorimeter. At this temperature the addendum contribution to the heat capacity is negligible. The nonzero x-axis intercept indicates that some of the ^{3}He is located outside of the calorimeter.

III. RESULTS AND DISCUSSION

All of the ^{3}He (<5 ppm ^{4}He) heat-capacity data presented in this paper were obtained in the vicinity of the pressure-dependent superfluid transition and have a precision of better than 1%. The temperature range of the measurements was 0.6—5 mK; the pressure range was 0 (i.e., vapor pressure) to 34 bars. Each of the samples was confined to constant density, which at these low temperatures also implies nearly constant pressure, using a valve mounted at low temperature. The cell pressure was continuously monitored using an *in situ* gauge. A list of pertinent parameters for each of the samples studied is given in Table II. Most of the specific-heat data, with various corrections applied, are plotted in Fig. 4. Figure 4(a) shows the results obtained at vapor pressure with the cell 95% full. Other data, not shown in the figure, were also obtained at vapor pressure but with less ^{3}He in the cell. These four sets of $P=0$ data will be discussed first.

A. Determination of the temperature scale

Precise, very-low-temperature heat-capacity measurements can be used to provide important input towards determining the thermodynamic temperature scale if the correct temperature dependence of the heat capacity is known *a priori*. For the case of liquid ^{3}He, the Landau theory yields the general result that the specific heat of the normal phase is proportional to the temperature, for temperatures small compared to the Fermi temperature $T_F\approx 1$ K. In this subsection we discuss our temperature scale which was determined partly by the constraint of this physical relation for the specific heat. The new scale is significantly different from the various scales currently being used. In particular, we find that along the melting curve the superfluid transition temperature (i.e., T_A) is 2.49 mK. This violates the previous consensus that T_A should be near the middle of the range 2.6—2.8 mK. However, if we accept the new determination of T_A, then the very serious discrepancies between previous measurements of the ^{3}He specific heat can be explained. There will naturally also be serious consequences for many other low-temperature measurements.

The heat-capacity measurements were made using an LCMN thermometer as discussed in Sec. II B. Equation (1) gives the relation between temperature and bridge ratio. Again, A, B, and Δ are calibration constants. The parameters were determined using bridge readings obtained at only three points: $T_c(0)$, T_A, and T_W. $T_c(0)$ is the ^{3}He superfluid transition temperature at zero pressure, and T_W is the superconducting transition temperature of tungsten. $T_c(0)$ was accurately located by the sharp kink in the warming curve of the partially filled cell. T_A was located using the melting-curve thermometer joined to the cell via the superconducting heat switch. The warming curve, as monitored by the MC thermometer, exhibited a kink at T_A. Steady-state comparisons between the LCMN and MC thermometers were made with the tem-

TABLE II. Some parameters of the ^{3}He samples studied.

Sample	P (bars)	V (cm^3)	Number of moles	T_c (mK)	$T_{A\text{-}B}$ (mK)	C_n/RT (K^{-1})	$(C_<-C_>)/C_>$ B	A
1	0	36.837	0.153	0.929				
2	0	36.837	0.230	0.929				
3	0	36.837	0.322	0.929				
4	0	36.837	0.435	0.929		2.78	1.46	
5	2.180	34.622	0.478	1.203		2.94	1.54	
6	5.209	32.469	0.510	1.495		3.11	1.61	
7	10.253	30.260	0.547	1.842		3.38	1.70	
8	14.950	28.904	0.573	2.067		3.63	1.76	
9	20.295	27.693	0.598	2.247		3.89	1.83	
10	25.307	26.806	0.618	2.364	2.183	4.12	1.89	1.94
11	29.079	26.284	0.630	2.427	2.081	4.32	1.91	1.99
12	33.953	25.585	0.647	2.486	1.940	4.54	1.97	2.12

perature being held fixed slightly below T_A and then slightly above T_A. The LCMN reading at T_A was determined by interpolation using these two thermometer comparisons along with the MC-thermometer reading at the transition. This LCMN-thermometer bridge reading agreed extremely well with the reading obtained later in the experimental run by filling the cell to near melting pressure and locating T_A with the LCMN thermometer directly. The calibration at T_W was made using the melting-curve thermometer as a transfer standard.[14]

If it were possible now to simply assign accurately known temperatures to each of the three transitions, the

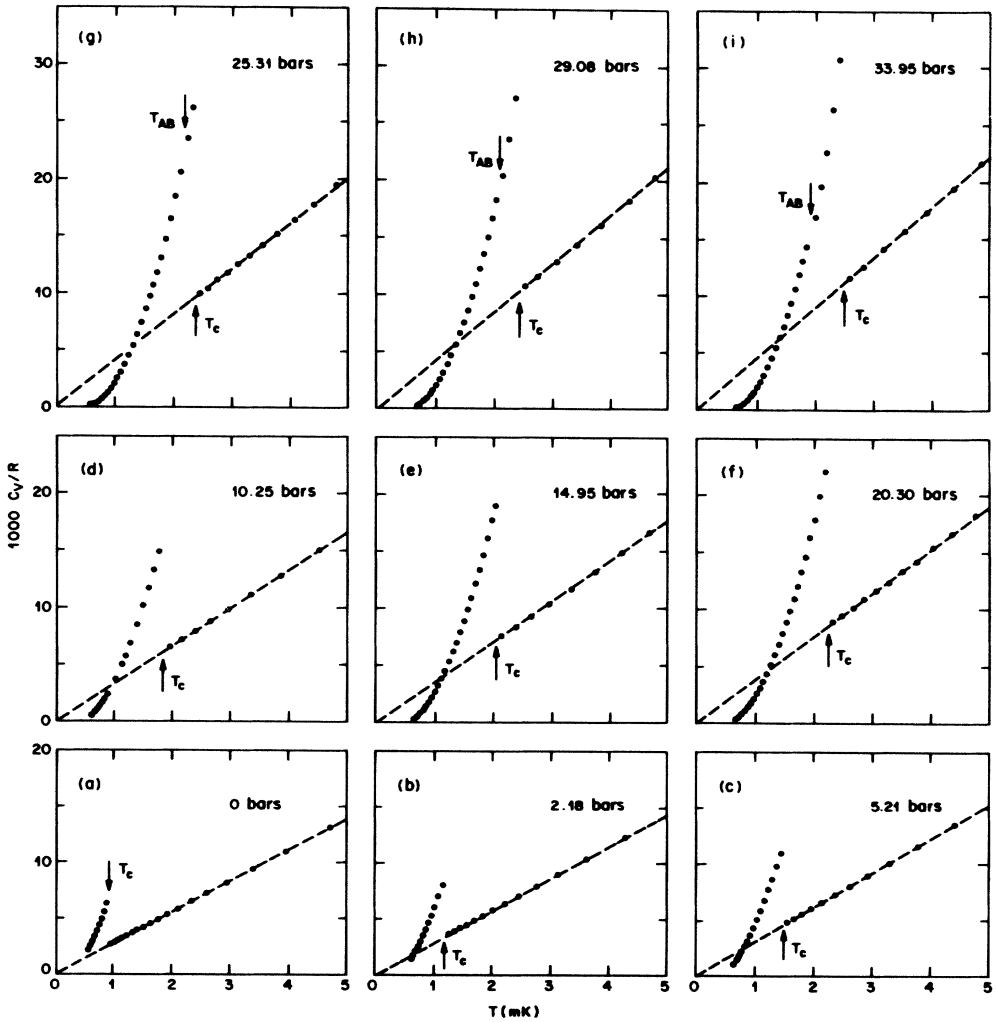

FIG. 4. ^{3}He specific heat, in units of the gas constant, plotted versus the temperature.

calibration of the LCMN thermometer, and therefore also the heat-capacity results, would be unambiguously determined. Unfortunately, we know only T_W sufficiently well; the National Bureau of Standards value[12] is 15.57±0.05 mK. We are forced then into allowing the adjustment of both T_A and $T_c(0)$, but under several important constraints: (i) the implied normal-phase specific heat measured using the LCMN thermometer must be linear in T, (ii) C/T must be equal to the value determined from higher-temperature C_V measurements, and (iii) the addendum heat capacity, measured with the cell partially filled, must be independent of the amount of ^{3}He in the cell.

In Figs. 5(a)—5(c) we show normal-phase specific-heat results obtained at $P=0$. Each of the fifteen curves corresponds to the same set of raw data but analyzed using different thermometer calibrations. Since the scatter in each string of data is small we show only the smooth curves drawn through the points. The curves grouped in Fig. 5(a) are based on calibrations with $F \equiv T_A/T_c(0) = 2.50$. In Figs. 5(b) and 5(c), F is equal to 2.60 and 2.70, respectively. This range for F brackets the various values extracted for this ratio from previous experiments,[1,3,28–32] see Table III. In Table III, T_S is the magnetic transition temperature for solid ^{3}He at melting pressure. $T_A/T_c(0)$ and T_A/T_S are listed separately in the table, but since[14] $T_c(0)$ is quite accurately equal to T_S, the two ratios should also be numerically the same. In the following discussion no distinction is made between the two ratios. The dashed straight horizontal lines in Figs. 5(a)—5(c) at $\gamma = c/nRT = 2.78\ \mathrm{K}^{-1}$ indicate the expected behavior for the $P=0$ specific heat. The γ value is from Ref. 8 with the correction applied in Ref. 14.

Obviously none of the curves in Fig. 5 is a straight line with zero slope; moreover, each has a low-temperature tail switching from negative going to positive going at $F \approx 2.55$. Similar sets of curves plotted using data obtained with progressively less ^{3}He in the cell show that the crossover occurs for smaller and smaller values of F. The conclusion is that there is a measurable addendum contribution to the heat capacity which increases with decreas-

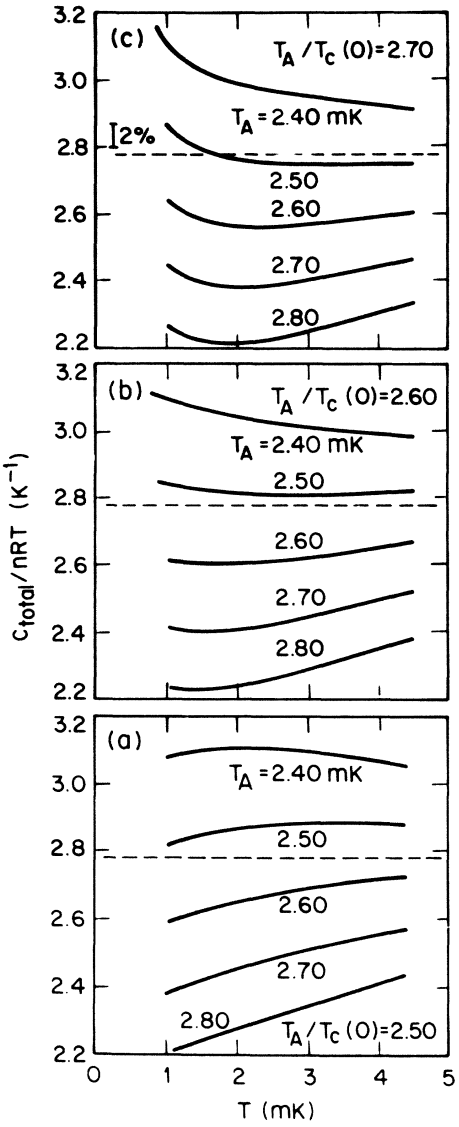

FIG. 5. Total, $P=0$, normal-phase heat capacity ($n=0.435$ moles) plotted for 15 different thermometer calibrations. Details are given in the text.

TABLE III. Measured temperatures for special points on the ^{3}He phase diagram.

	T_A (mK)	$T_A/T_c(0)$	T_A/T_S	Thermometry
Halperin *et al.*[a]	2.75±0.11		2.50±0.05	Latent heat of melting
Kummer *et al.*[b]	2.68±0.21		2.60	Latent heat of melting
Paulson *et al.*[c]	2.62	2.49		LCMN
Avenel *et al.*[d]	2.75±0.05		2.55	Pt NMR
Haavasoja *et al.*[e]	2.79±0.14	2.68		Pt NMR
Osheroff and Yu[f]			2.67	Pt NMR
Osheroff[g]		2.69±0.01		Pt NMR
This work	2.49±0.02	2.68±0.03		LCMN

[a]Reference 3.
[b]Reference 28.
[c]Reference 31. $\Delta_{LCMN} \equiv 0$.
[d]Reference 32.
[e]Reference 1.
[f]Reference 29.
[g]Reference 30. The value tabulated is extrapolated from measurements at 0 and 29 bars pressure.

ing temperature. Therefore F must be greater than 2.55. If we temporarily ignore the data which are obviously affected by the addendum contribution, i.e., the data below ~ 2 mK, then it is evident from the figure that, for any value of F, c/nRT is independent of temperature only if $T_A \approx 2.5$ mK. If we insist that γ be approximately equal to 2.78, then we find that F must be in the range 2.6—2.7, which is consistent with our first estimate.

More quantitative statements about both F and T_A can be made if the addendum heat capacity at $P=0$ is considered in more detail. We note first that since the addendum may be due to a surface contribution, only partial fillings of the cell were considered which were sufficient to completely submerge the sintered-silver heat exchanger and the LCMN thermometer. With this provision then, the addendum heat capacity should be independent of sample size. We therefore searched for values of F and T_A which would yield this result.

The addendum heat capacity computed for each temperature calibration and for each partial filling of the cell was determined using

$$c_{\rm ad}(F,T_A,n,T)=c_{\rm total}(F,T_A,n,T)-nR\gamma T \ . \qquad (3)$$

In the computations γ was taken to be 2.78 $\rm K^{-1}$, which means that F and T_A were not independent quantities. It was therefore necessary to determine first, for a given value of F, the value of T_A which yielded $c_{\rm total}/nRT=\gamma$ for $T \gtrsim 2.5$ mK. This was done by constructing plots similar to Fig. 5. It was then straightforward to compute the addendum heat capacity for each partial filling corresponding to this particular set of F and T_A. Plotted in Fig. 6, as a function of F and at a temperature of 0.95 mK, is the difference between the addendum heat capacities determined for the smallest and largest partial fillings of the cell. The error bars indicate only the precision of the difference determinations. The zero crossing occurs at $F=2.675\pm0.015$. Allowing for a 1% uncertainty in γ and for a 0.05-mK error in $T_{\rm W}$, we obtain our final results,

$$F=2.68\pm0.03, \quad T_A=2.49\pm0.02 \text{ mK} \ . \qquad (4)$$

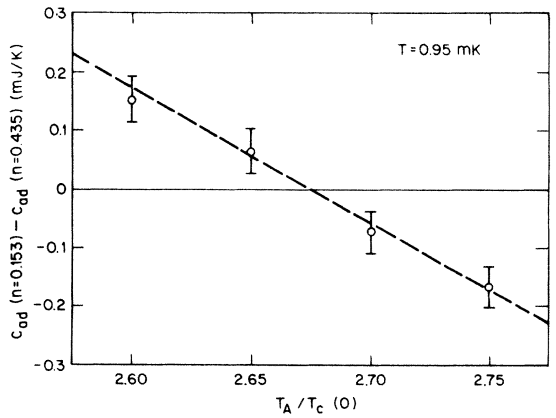

FIG. 6. Difference in the apparent addendum heat capacities for two partial fillings of the calorimeter plotted for several thermometer calibrations. The addendum is independent of the amount of ^{3}He in the cell if $T_A/T_c(0)=2.68$.

Comparison with determinations from several other groups is made in Table III.

The new determination of F agrees extremely well with the more recent Pt NMR results.[1,29,30] However, the new value of T_A, which pins our scale to absolute temperatures, is considerably smaller than any of the listed values. This difference has serious consequences. The particular implications in regard to the ^{3}He specific heat will be discussed in Sec. III C.

Figure 7 shows the addendum heat capacity determined for all four partial fillings of the cell based on F and T_A given by Eq. (4). There is no systematic dependence on the number of moles of ^{3}He in the cell.

Figure 8 shows the same four sets of data plotted in a different manner. We now have $c_{\rm total}/nRT$ versus T, which shows that the precision of the data is better than 1% and also that the addendum is less than 4% of the total heat capacity for $n=0.435$ moles. The coincidence of the curves near 4 mK indicates that the number of moles of sample is known to better than $\frac{1}{2}$%.

Detailed comparisons are made with two particular temperature scales: the scale of Haavasoja and co-workers (Ref. 1) and the scale of Paulson *et al.* (Ref. 31). A common connection between these two scales and our own is that LCMN thermometers were employed. The Δ [see Eq. (1)] for our LCMN thermometer, based on $F=2.68$ and $T_A=2.49$ mK, was -0.121 mK. Haavasoja and coworkers found that the Δ for their thermometer (3 at.% CMN) was on various cooldowns between -0.11 and -0.13 mK. Their values were obtained from calibrations against a Pt NMR thermometer for temperatures in the range 0.7—10 mK. The NMR thermometer gave $F=2.68$. Absolute temperatures were derived from measurements of the spin-lattice relaxation time using the Korringa relation $\tau_1 T=K_{\rm Pt}$ with $K_{\rm Pt}=29.9$ msec K.[33] They found $T_A=2.79$ mK. If we assume that $T_A=2.49$ mK is the correct temperature and adjust their T scale by the factor $2.49/2.79=0.892$, then the corrected Δ's lie in the range -0.10 to -0.12 mK. These values remain in excellent agreement with our Δ. We note further that, aside from a scaling factor, the T^* scale (i.e., $\Delta\equiv0$) of Ref. 1 agrees[1,14] well with the magnetic temperature scale (5 at.% CMN) of Ref. 31. This means that our T^* scale should also be proportional to this latter scale. Our values

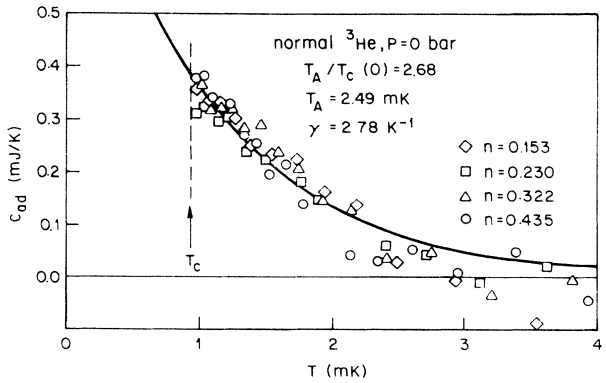

FIG. 7. Addendum heat capacity plotted for four partial fillings of the calorimeter.

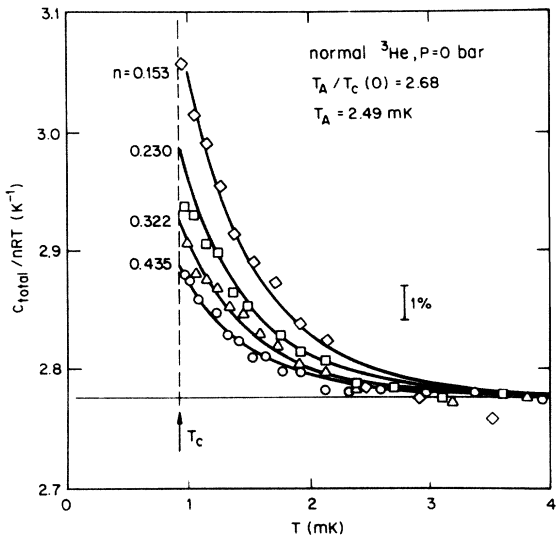

FIG. 8. Total heat capacity (i.e., sample plus addendum) divided by nRT plotted for four partial fillings of the cell.

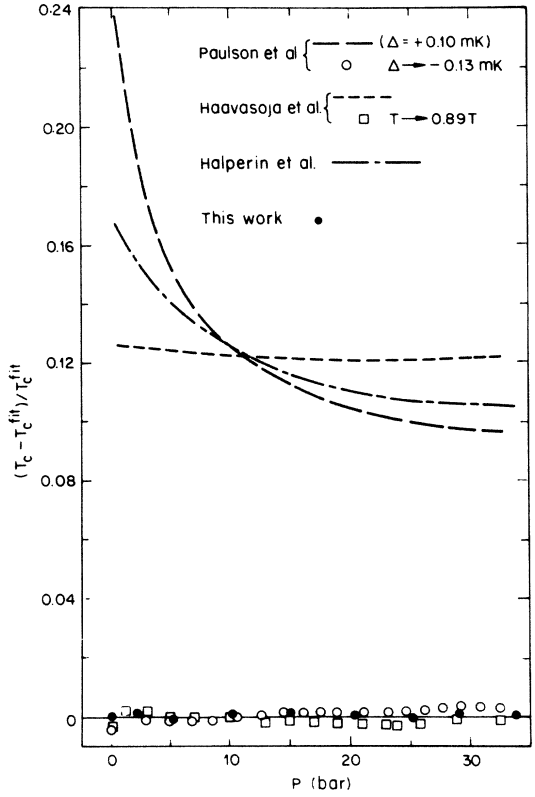

FIG. 9. Deviations from the transition line between normal and superfluid ^{3}He described by Eq. (5).

of F^* and T_A^* are 2.49 and 2.61 mK, respectively; the values of Ref. 31, from Table III, are 2.49 and 2.62 mK. We have then more than just proportionality; these two T^* scales are essentially identical. We thus find that the LCMN thermometers used by Haavasoja and co-workers,[1] by Paulson *et al.*,[31] and by us all behave in a very similar fashion; the discrepancies in the absolute-T scales are due only to the differences in thermometer calibration. An important corollary is that the simple expression, Eq. (1), can be used to accurately relate temperature and LCMN susceptibility even for temperatures extending below 1 mK. This follows from the careful and detailed comparisons made against the Pt NMR thermometer of Ref. 1.

The present T_c-versus-P data are described well by the empirical relation

$$T_c = \sum_{i=0}^{5} a_i P^i , \tag{5}$$

with

$$a_0 = 0.929\,383\,75, \quad a_1 = 0.138\,671\,88 ,$$

$$a_2 = -0.693\,021\,85 \times 10^{-2}, \quad a_3 = 0.256\,851\,69 \times 10^{-3} ,$$

$$a_4 = -0.572\,486\,44 \times 10^{-5}, \quad a_5 = 0.530\,109\,18 \times 10^{-7} .$$

T_c is in mK; P is in bars. The deviations from this best fit are plotted as solid circles in Fig. 9. The rms deviation is 0.06%. A listing of smoothed P, T_c values is given in Table IV. The long-dashed curve in Fig. 9 shows the $T_c(P)$ results determined by Ref. 31. Changing their Δ from $+0.100$ to -0.130 mK results in the data points plotted as open circles. The short-dashed curve shows the results of Ref. 1. Scaling their temperatures by the factor 0.89 results in the points plotted as open squares. Over the entire pressure range both sets of corrected T_c's agree with the present results to within better than $\frac{1}{2}$%.

The fact that our temperature scale differs from the scale of Ref. 1 simply by an overall scaling factor is reassuring since that scale is based on Pt NMR thermometry, which we expect, barring experimental difficulties, to give *relative* temperatures correctly. The fact that the difference between the scale of Ref. 31 and our scale is due only to a constant temperature shift is reassuring too since in their work it is T^* which should be determined

TABLE IV. Pressure-temperature coordinates for the transition between normal and superfluid ^{3}He. The smoothed values were computed using Eq. (5).

P (bars)	T_c (mK)	P (bars)	T_c (mK)
0	0.929	18	2.177
1	1.061	19	2.209
2	1.181	20	2.239
3	1.290	21	2.267
4	1.388	22	2.293
5	1.478	23	2.317
6	1.560	24	2.339
7	1.636	25	2.360
8	1.705	26	2.378
9	1.769	27	2.395
10	1.828	28	2.411
11	1.883	29	2.425
12	1.934	30	2.438
13	1.981	31	2.451
14	2.026	32	2.463
15	2.067	33	2.474
16	2.106	34	2.486
17	2.143	34.338	2.491

with little ambiguity. We therefore do not contradict the real basis of either of these thermometry techniques. Nevertheless, our absolute scale is significantly different from both.

It is interesting to note that the 1974 scale of Ahonen *et al.*[34] gives temperatures which are systematically lower than the new scale of Haavasoja and co-workers[1] by $\sim 10\%$ and therefore is in quite good agreement with the temperature scale we are proposing in this paper. The 1974 scale was also based on Pt NMR and was calibrated using a Korringa constant of 29.8 msec K. Above 5 mK the platinum thermometer was compared against a nuclear orientation thermometer. It was stated later,[33] however, that there was a 10% calibration error in the time base of the pulsed NMR spectrometer. Presumably this must have been accompanied by an error of comparable magnitude in the nuclear orientation thermometry.

The dashed-dotted curve in Fig. 9 corresponds to the melting-curve temperature scale of Halperin *et al.*[3] (also see the Appendix). The mapping of this scale onto the superfluid transition line was performed using Eq. (5) of Ref. 14. This best-fit equation relates sample pressure to melting-curve pressure measured at the temperature of the superfluid transition. In principle, the temperature scale of Halperin *et al.*, which is based on latent-heat measurements, should be at least proportional to the thermodynamic temperature. Consequently, the dashed-dotted curve plotted in Fig. 9 should parallel the curve of Haavasoja *et al.* Obviously, there is a serious inconsistency. We speculate, prejudiced primarily by the fact that our new scale is proportional to this scale and also by the fine agreement between the most recent NMR experiments, that the problem lies with the results of Halperin *et al.*

It is interesting, although any significance is not immediately obvious, that the expression

$$T_{\text{new}} = 0.954 T_{\text{Halperin}} - 0.130 \text{ mK} \tag{6}$$

quite accurately relates our scale and the scale of Halperin *et al.*

Further discussion of the temperature scale is deferred until after the specific-heat results have been presented.

B. Addendum heat capacity

This subsection continues the discussion of the addendum heat capacity which played a role in determining our temperature scale (Sec. III A). The addendum extracted from the $P=0$ measurements and for $T > T_c$ is shown in Fig. 7. This excess heat capacity may be due to a contribution from the portion of the ^{3}He sample very near the surface of the silver sinter, but a simple background contribution from the calorimeter itself cannot be ruled out. Because of the small size of the addendum relative to the total heat capacity, the scatter in the points plotted in Fig. 7 is rather large and this prevents an unambiguous determination of the temperature dependence of this term. We do find though, that the equation

$$c_{\text{ad}} = a e^{-T/b} , \tag{7}$$

with $a = 1.0$ mJ/K and $b = 1.0$ mK, describes the data reasonably well. The curves drawn in both Figs. 7 and 8 were computed using this relation. We note that our addendum heat capacity is roughly a factor of 4 smaller than that found by Haavasoja and co-workers[1] from very similar measurements. Both their calorimeter and our own had estimated surface areas of 10 m^2. However, their surface area was determined using an electron microscope while ours was determined from BET measurements. It is therefore conceivable, because of the very different techniques, that the two surface areas are really quite different. So it remains possible that the addendums in both experiments result from surface contributions.

The extraction of the addendum heat capacity from the experimental data obtained below $T_c(0)$ is more involved. The complication is due to the suppression of the superfluid phases near surfaces. Following Haavasoja and coworkers,[1] we write, for $T < T_c$,

$$c_{\text{total}} = n_s C_s + n_n C_n + c_{\text{ad}} , \tag{8}$$

where C_s and C_n are the molar specific heats of the superfluid and normal phases, respectively. We assume that n_n is proportional to ξ, the coherence length, and is therefore temperature dependent. With the definition

$$\Delta C(T) \equiv C_n(T) - C_s(T) \tag{9}$$

and $n = n_s + n_n$, Eq. (8) can be rewritten as

$$c_{\text{total}}(T,n) = n C_s(T) + n_n(T) \Delta C(T) + c_{\text{ad}}(T) . \tag{10}$$

Thus if for a given temperature c_{total} is plotted versus n, the data will fall on a straight line with slope equal to $C_s(T)$ and intercept given by the last two terms of Eq. (10). These intercepts, which have an uncertainty of about 0.1 mJ/K, are plotted as a function of temperature in Fig. 10. Note that above T_c [see Eq. (8)], $n_s \equiv 0$ and the intercept gives c_{ad} directly. The values for $T > T_c$ determined using this procedure agree well with those from the first method (Sec. III A); the curve which has

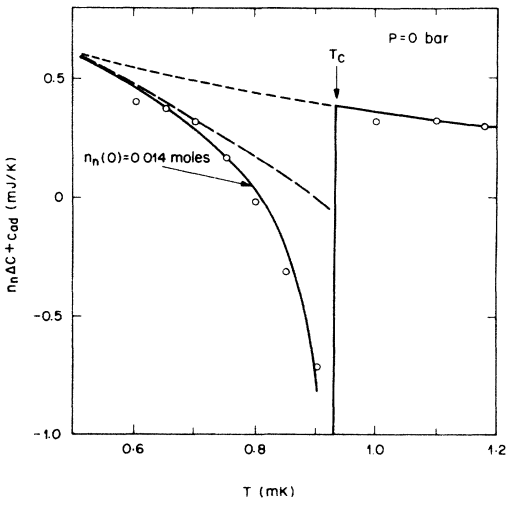

FIG. 10. Apparent addendum heat capacity. The step at T_c shows that a portion of the ^{3}He sample remains normal below T_c. Details are given in the text.

been drawn solid above T_c and dashed below T_c corresponds to Eq. (7). Obviously, if none of the liquid remained normal below T_c, there would be no discontinuity at T_c. The solid curve which quite accurately describes the $T<T_c$ values was computed assuming that Eq. (7) describes c_{ad} even for $T<T_c$ and using

$$n_n(T)=n_n(0)\left[1-\left[\frac{T}{T_c}\right]^4\right]^{-1/2}, \tag{11}$$

with $n_n(0)=0.014$ mole. The long-dashed curve results if it is assumed that n_n is temperature independent and equal to 0.014 mole. The second factor in Eq. (11) is the Gorter-Casimir approximation for the temperature dependence of the penetration depth of a superconductor. It is assumed and consistent with the experimental results shown in Fig. 10 that $\xi(T)$ for superfluid ^{3}He behaves in a similar manner.

Our zero-temperature value for n_n corresponds to a layer of normal liquid covering the silver sinter which is about 500 Å thick. The zero-temperature coherence length, given by

$$\xi_0=\hbar v_F/\pi k_B T_c , \tag{12}$$

is equal to 1400 Å at $P=0$. Thus our finding is that $l_n(T)\approx\frac{1}{3}\xi_0$ which seems reasonable. At $T=0.95T_c$, $l_n\approx 1200$ Å. This thickness can be compared with the estimated[19] average pore diameter in the sinter of 5000 Å.

In their work, Haavasoja and co-workers assumed that l_n was temperature independent and from measurements *near* T_c determined that $l_n\approx 500$ Å. This is more than a factor of 2 different from our result. If the surface area of their calorimeter was actually larger than ours, as conjectured earlier in this subsection, the discrepancy would be increased.

The following is a discussion of our procedure for treating the heat-capacity data obtained at $P>0$. Since it is possible that the addendum is due, at least in part, to a surface contribution, there may be a pressure dependence to this term. The evidence, though, is that any pressure dependence must be quite mild: At high pressure and at the lowest temperature the total heat capacity measured becomes very small (see Fig. 4); in fact, it becomes comparable to c_{ad} given by Eq. (7). Using Eq. (7) in our analysis of the $P>0$ data leads to a superfluid specific heat which behaved qualitatively as expected down to our lowest temperature. We thus conclude that c_{ad} increases by no more than 20% between 0 and 34 bars. This uncertainty in the pressure dependence of c_{ad} has an insignificant effect on most of the specific-heat data.

Below $T_c(P)$ it was assumed, as in the experiment of Haavasoja and co-workers, that the thickness of the normal layer has the same pressure dependence as ξ_0. Therefore n_n is proportional to $\xi/V\propto 1/\gamma T_c V^{2/3}$. V is the molar volume [see Eq. (2)]. The complete expression for C_s is

$$C_s(P,T)=[c_{\text{total}}(P,T)-c_{ad}(T)-n_n(P,T)\gamma(P)RT]\times[n-n_n(P,T)]^{-1} , \tag{13}$$

with

$$n_n(P,T)=\left[\frac{V(0)}{V(P)}\right]^{2/3}\frac{\gamma(0)}{\gamma(P)}\frac{T_c(0)}{T_c(P)}\times 0.014\left[1-\left[\frac{T}{T_c}\right]^4\right]^{-1/2} . \tag{14}$$

C. *A-B* Transition

Before presenting the specific-heat results, we discuss our determination of $T_{A\text{-}B}(P)$ and also our measurement of the latent heat at this first-order transition. The latent heat provides a means of comparing energy measurements in different specific-heat experiments that is completely independent of temperature scale.

The measurements were performed by dissipating a small amount of power in the cell heater and by carefully monitoring the temperature of the cell as it slowly drifted through the region of the *A-B* transition. Figure 11 shows a tracing obtained at $P=33.95$ bars.

The time interval over which the temperature does not change corresponds to the coexistence of the *A* and *B* phases in the calorimeter. As the pressure is lowered the latent heat becomes progressively smaller. The lowest pressure at which we could clearly detect the *A-B* transition was 23 bars. At each pressure some superheating of the transition was evident, but it was always small (<1 μK) and did not seriously affect the precision of the $T_{A\text{-}B}$ measurement.

The transition temperatures are described well by the equation

$$T_{A\text{-}B}=T_{\text{PCP}}+\sum_{i=1}^{5} a_i(P-P_{\text{PCP}})^i , \tag{15}$$

with $P_{\text{PCP}}=21.22$ bars, $T_{\text{PCP}}=2.273$ mK, and

$a_1=-0.103\,226\,23\times10^{-1}$, $a_2=-0.536\,331\,81\times10^{-2}$,

$a_3=0.834\,370\,32\times10^{-3}$, $a_4=-0.617\,097\,83\times10^{-4}$,

$a_5=0.170\,389\,92\times10^{-5}$.

P_{PCP} is the pressure of the polycritical point determined by Paulson *et al.*[35] and T_{PCP} is T_c at P_{PCP} determined using Eq. (5). The ^{3}He phase diagram based on Eqs. (5)

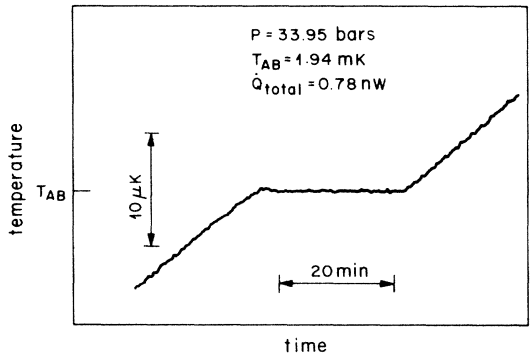

FIG. 11. Temperature recorded by the LCMN thermometer as the calorimeter was slowly warmed through the *A-B* transition.

and (15) is given in Fig. 12. Deviations of the $T_{A\text{-}B}$ values from Eq. (15) are plotted in Fig. 13. Also plotted are the data of Haavasoja and co-workers scaled by 0.89 and the data of Paulson *et al.*[31] assuming $\Delta_{LCMN}=-0.13$ (see Sec. II B). Equation (15) describes all three sets of data to within 0.2%. A listing of smoothed values is given in Table V.

The latent heat at $T_{A\text{-}B}$ is given by

$$L_{A\text{-}B}=\dot{Q}\,\Delta t/n\ , \tag{16}$$

where $\dot{Q}$ is the total rate of heat input to the cell and Δt is the time necessary to warm through the two-phase region. Note that the temperature scale does not enter into this expression. It would appear that the latent heat could be measured in a very straightforward manner. However, $L_{A\text{-}B}$ is quite small, which means that $\dot{Q}$ must also be small. Consequently, the residual heat leak into the cell has to be accurately accounted for. This was accomplished by determining $\dot{Q}$ via the relation $\dot{Q}=c\dot{T}$. Each latent-heat datum point thus results from measurements of c, $\dot{T}$, and Δt. $L_{A\text{-}B}$ is plotted as a function of pressure in Fig. 14. The error bars correspond to a 1% uncertainty in c and $\dot{T}$ and an uncertainty in Δt of 30 sec. These new results for $L_{A\text{-}B}(P)$ agree extremely well with the latent heat measured by Halperin *et al.*[3] at melting pressure. We also find agreement with the results of Haavasoja and co-workers, to within the combined experimental uncertainty, except for their point at 32.5 bars. Because their values are systematically smaller than ours, however, we conclude that there must be at least a small difference in our energy determinations. Therefore even if the temperature scale of Haavasoja and co-workers is brought into agreement with our scale we still expect their specific-heat values to be a few percent smaller.

D. Normal-phase specific heat

The results for the specific heat of normal ^{3}He are plotted as $C/RT\equiv\gamma$ versus T in Fig. 15. At each pressure, γ is temperature independent to within the precision of the data. This condition was imposed on the $P=0$ data as a constraint in the determination of the temperature scale

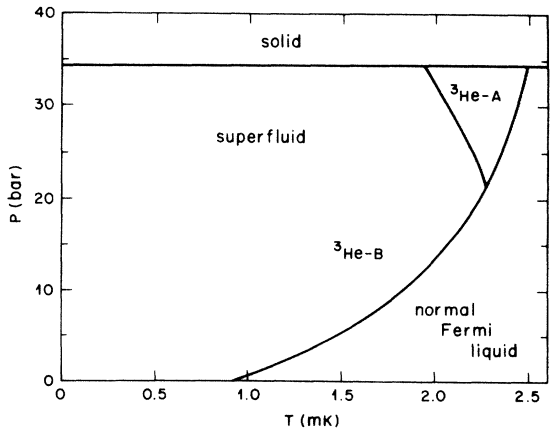

FIG. 12. ^{3}He phase diagram determined by Eqs. (5) and (15).

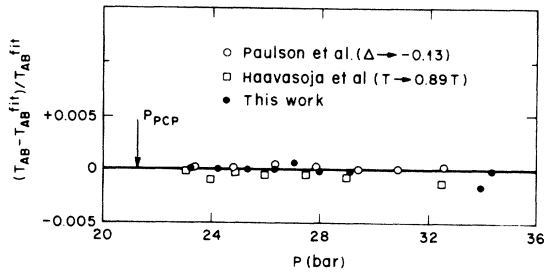

FIG. 13. Deviations from the A-B transition line described by Eq. (15).

(Sec. II A), but based on the results of Haavasoja and co-workers there was no guarantee that this would remain true at higher pressures. Haavasoja and co-workers[1] reported an anomalous contribution to the normal specific heat for sample pressures less than 10 bars. The anomalous contribution increased with decreasing temperature and at $P=0$ accounted for approximately 10% of the total specific heat near 1 mK. They concluded that this excess term was a property of bulk liquid ^{3}He. If this were indeed true, then our temperature-scale determination would be invalid, since our basic premise is that the $P=0$ specific heat is linear in T. Had we imposed this condition artificially, our data at $P>0$ would have shown anomalous behavior, which is not the case. Our measurements thus contradict their finding. Since our relative temperature scales are identical, we can also conclude that the anomaly is not due to temperature-scale problems. Further support for the absence of an anomalous contribution at very low temperatures comes from the specific-heat measurements by Zeise *et al.*[2] The temperature scale used in Ref. 2 for this experiment was identical to the scale of Haavasoja and co-workers.

Figure 16 shows the averaged γ values plotted as a function of the sample pressure. The solid circles are the new results; the open circles are our previous values[8] in-

TABLE V. Pressure-temperature coordinates for the A-B transition in superfluid ^{3}He. The smoothed values were computed using Eq. (15).

P (bars)	$T_{A\text{-}B}$ (mK)
21.22	2.273
22	2.262
23	2.242
24	2.217
25	2.191
26	2.164
27	2.137
28	2.111
29	2.083
30	2.056
31	2.027
32	1.998
33	1.969
34	1.941
34.358	1.932

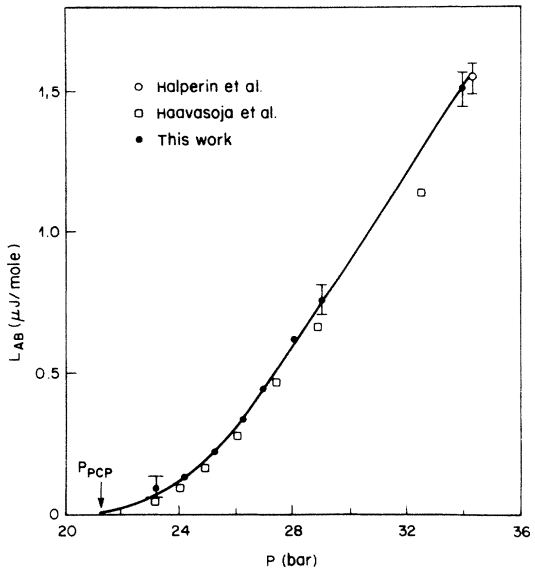

FIG. 14. Pressure dependence of the latent heat at the A-B transition.

creased by[14] $1\frac{1}{2}\%$ to account for the recent revisions in the NBS temperature scale. Again the agreement at $P=0$ was a constraint used in the determination of our temperature scale. We find that excellent agreement persists over the entire pressure range. The solid curve which fits the data corresponds to the expression

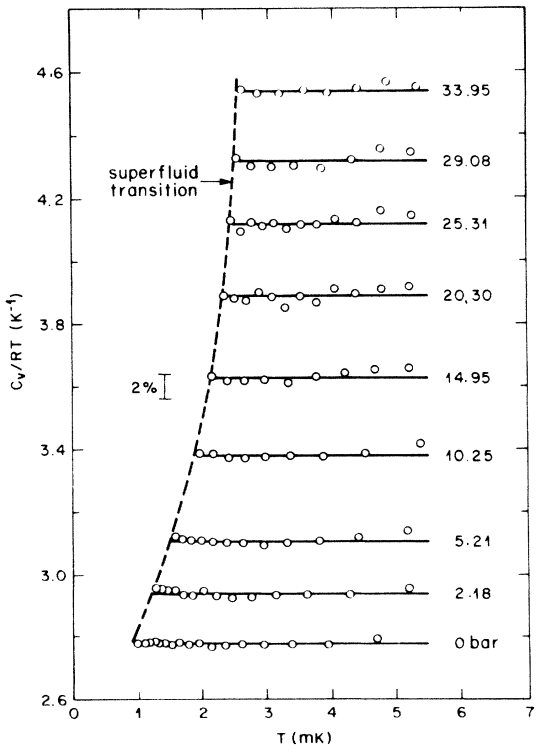

FIG. 15. Normal-phase specific heat of ^{3}He plotted as C/T versus T. The numbers give the sample pressures in bars.

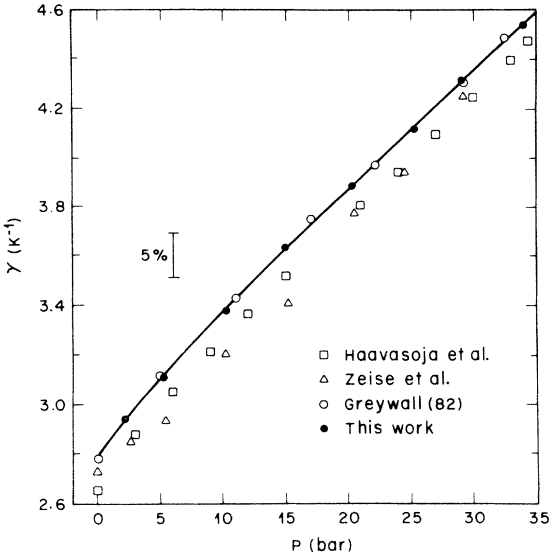

FIG. 16. Comparison of γ values derived from normal-phase specific-heat measurements. The points attributed to Haavasoja and co-workers (Ref. 1) and Zeise *et al.* (Ref. 2) are corrected values; see text.

$$\gamma(P)=\sum_{i=0}^{4} a_i P^i , \tag{17}$$

with

$a_0=0.278\,404\,64\times10^{1}$, $a_1=0.695\,752\,43\times10^{-1}$,

$a_2=-0.147\,383\,03\times10^{-2}$, $a_3=0.461\,534\,98\times10^{-4}$,

$a_4=-0.537\,853\,85\times10^{-6}$.

Some smooth values are listed in Table VI.

In Ref. 8 a detailed comparison was made between the earlier specific-heat results, the differences between the various previous measurements being as large as 40%. It was demonstrated, however, that only the results presented in Ref. 8 satisfied several important thermodynamic consistency checks. The γ values determined in Ref. 1 and in Ref. 2 fell systematically more than 20% below those results[8] at all pressures. More recent measurements have been made by Mayberry, Fogle, and Phillips[9] at vapor pressure for $15\lesssim T\lesssim 150$ mK and by Sen and Archie[10] at 0.13 and 28.5 bars for $20\lesssim T\lesssim 350$ mK. Both of these sets of data agree well with our higher-temperature results presented in Ref. 8. Indirect support also comes from the theoretical work of Levin and Valls.[11]

The γ values attributed to Haavasoja and co-workers[1] and also to Zeise *et al.*[2] in Fig. 16 are their actual data multiplied by the factor $(1/0.89)^2$. This correction corresponds to their temperature scale being adjusted by the factor 0.89 (see Sec. III A) which brings their temperature scale into coincidence with ours. The corrected γ values are in quite good agreement with the present results. The values of Haavasoja and co-workers remain systematically below ours by a few percent, but this can be attributed to the differences in our energy measurements discussed in Sec. II C. It should be noted that the γ values of Haavasoja and co-workers for $P\lesssim 10$ bars were deter-

TABLE VI. Parameters derived from the smoothed normal-phase specific-heat results.

P (bars)	V (cm^3)	γ (K^{-1})	m_3^*/m_3	F_1^S
0	36.84	2.78	2.80	5.39
1	35.74	2.85	2.93	5.78
2	34.78	2.92	3.05	6.14
3	33.95	2.98	3.16	6.49
4	33.23	3.04	3.27	6.82
5	32.59	3.10	3.38	7.14
6	32.03	3.16	3.48	7.45
7	31.54	3.21	3.58	7.75
8	31.10	3.27	3.68	8.03
9	30.71	3.32	3.77	8.31
10	30.35	3.37	3.86	8.57
11	30.02	3.42	3.95	8.84
12	29.71	3.48	4.03	9.09
13	29.42	3.53	4.12	9.35
14	29.15	3.58	4.20	9.60
15	28.89	3.62	4.28	9.85
16	28.64	3.67	4.37	10.10
17	28.41	3.72	4.45	10.35
18	28.18	3.77	4.53	10.60
19	27.96	3.82	4.61	10.84
20	27.75	3.87	4.70	11.09
21	27.55	3.92	4.78	11.34
22	27.36	3.97	4.86	11.58
23	27.18	4.02	4.94	11.83
24	27.01	4.06	5.02	12.07
25	26.85	4.11	5.10	12.31
26	26.70	4.16	5.18	12.55
27	26.56	4.21	5.26	12.79
28	26.42	4.26	5.34	13.03
29	26.29	4.31	5.42	13.26
30	26.17	4.36	5.50	13.50
31	26.04	4.40	5.58	13.73
32	25.90	4.45	5.66	13.97
33	25.75	4.50	5.74	14.21
34	25.58	4.54	5.82	14.46
34.39	25.50	4.56	5.85	14.56

mined using data at sufficiently high temperatures where no excess specific heat was observed.

At melting pressure, Halperin *et al.*[3] found γ to be 4.33 K^{-1}. This value is based on a temperature scale which also differs considerably from ours, see Table III. The conversion of this value onto our new temperature scale was accomplished using the relation

$$\left[\frac{C}{T}\right]_{\text{new}} = \left[\frac{C}{T}\right]_{\text{old}} \left[\frac{1}{T}\frac{dP}{dT}\right]_{\text{new}} \Big/ \left[\frac{1}{T}\frac{dP}{dT}\right]_{\text{old}} \tag{18}$$

and a calibration of the melting curve based on the new scale (see the Appendix). The adjusted γ is 4.91, which is about 7% larger than our melting-curve value. This difference is somewhat larger than we might have expected; however, the measurements by Halperin *et al.*[3] are rather more involved than the standard specific-heat experiment and are complicated by the coexistence of liquid and solid ^{3}He in the cell. Furthermore, Halperin *et al.* made no correction for the background contribution of their Be-Cu cell.

The point that we wish to stress is that there are now three independent specific-heat experiments spanning the complete pressure range, which give essentially the same ^{3}He specific heat, provided the analysis is performed using the same temperature scale. This is very convincing evidence that there are no trivial errors in any of the three experiments; the differences in the reported values of γ must be due only to the difference in the temperature scales used. Furthermore, if the γ values from the higher-temperature experiments are correct, the very-low-temperature scale of Ref. 1, and indeed all other currently used very-low-temperature scales, must be seriously in error. The problem then switches over to finding possible sources for error in the older scales. A crucial input to the Pt NMR scale of Ref. 1 and also to the scale of Ref. 32 is the Korringa constant which fixes the absolute temperatures. This constant has been measured several times and these values agree to within a few percent, but this may be fortuitous since the Korringa constant is extremely sensitive to the level of magnetic impurities in the platinum. Richardson[36] has noted that some samples do not obey the Korringa law at all. Moreover, Paulson *et al.*[31] have noted that subsequent work by Varoquaux and coworkers on high-purity samples has shown that $K_{\text{Pt}} \equiv \tau_1 T$ is not constant but is field and temperature dependent. These effects could be responsible for considerable uncertainty in the scales of Refs. 1 and 32.

An experiment which was reported to verify the correctness of the temperature scale of Ref. 1 was performed by Lhota *et al.*[37] In this work the scale of Ref. 1 was compared with the NBS noise-and-nuclear-orientation scale using the superconducting transition temperatures of tungsten and beryllium samples as transfer standards. The Pt NMR thermometer was calibrated to give the Ref. 1 temperature for $T_c(0)$, namely 1.04 mK. With this normalization the NMR thermometer yielded a transition temperature ($\approx$24 mK) for the beryllium sample which agreed with the NBS value to within 0.2%; however, the transition temperature ($\approx$15 mK) of the tungsten sample located inside the experimental cell was 4.5% too high. No explanation was offered for the large discrepancy, but it was concluded that the two scales were in excellent agreement. We speculate that the discrepancy signals some serious problem. If the problem is not with the fixed-point readings, then their NMR thermometer does not obey a Curie relation in the vicinity of 20 mK. Our opinion is that a convincing statement about the scale of Ref. 1 at much lower temperature cannot be made based on this experiment. More generally, the existing body of thermometry data does not appear to rigorously exclude the temperature scale that we are proposing.

E. Superfluid specific heat

The superfluid specific-heat data obtained at a pressure of 20 bars are plotted logarithmically against the inverse

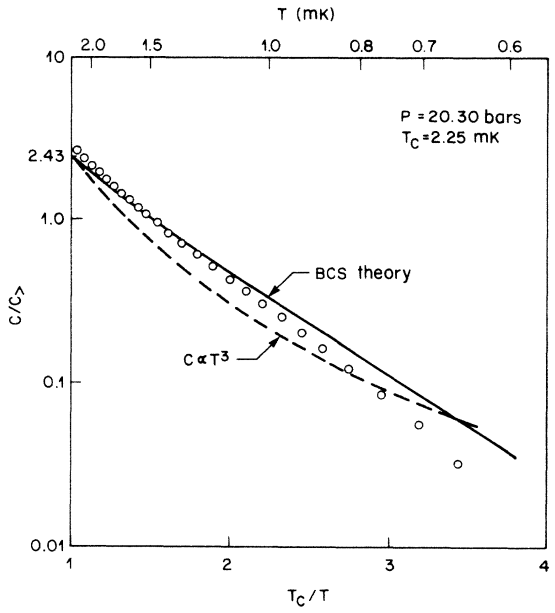

FIG. 17. B-phase specific heat of ^{3}He at 20.3 bars pressure. The measured specific heat has a temperature dependence which is similar to weak-coupling BCS theory and also to a simple T^3 behavior.

temperature in Fig. 17. This type of plot has been commonly used to present specific-heat data for superconductors. The fact that the data can be quite well described by a straight line with negative slope is indicative of a finite energy gap between the ground state and the lowest excited states of the system. The stronger temperature dependence near T_c results because the energy gap is temperature dependent and falls to zero at T_c. The specific heat calculated using the BCS theory is also shown in the figure. Over the entire temperature range the theoretical curve shows qualitatively the same features as the experimental data. There are, however, quantitative differences which increase with increasing sample pressure. The departures from BCS theory are attributed to strong-coupling effects. The dashed curve plotted in Fig. 17, which nearly parallels the data near T_c, corresponds to a specific heat which is proportional to T^3. Scaling the measured superfluid specific heat by the factor $1/T^3$ thus suppresses most of its temperature dependence.

Figure 18 shows the dimensionless quantity $(C_s/C_>)/(T/T_c)^3$ plotted versus T/T_c for all nine sample pressures. $C_>$ is the specific heat just above the transition, i.e., $C_n(T_c)$. The solid circles are B-phase data, the open circles A-phase data. The solid and long-dashed curves show theoretical results which will be discussed later. The extrapolation of the B-phase data up to T_c yields the values of the specific-heat jump $\Delta C/C_> \equiv (C_< - C_>)/C_>$ given in each panel of the figure. At $P=0$, $\Delta C/C_> = 1.46$, which is very close to the weak-coupling value 1.43. Therefore the data shown in Fig. 17(a) should closely follow the theoretical curve, which differs only slightly from the BCS specific heat. We attribute the deviations which set in for $T/T_c \lesssim 0.8$ ($T \lesssim 0.7$ mK) to experimental problems. It should be noted first that scaling the data by T^3 exaggerates possible errors in the temperature scale. Also, at very low temperatures the sample heat capacity becomes very small and, therefore, because of the faster drift rates, more difficult to measure. Moreover, the correction for the addendum (Sec. III B) which could not be directly measured below T_c becomes larger. Fortunately, as the pressure increases, T_c also increases, which means that the onset for the more rapid growth in the experimental uncertainty shifts to lower and lower relative temperatures. Consequently, the data, as a function of reduced temperature, are most reliable for the higher-pressure samples where the strong-coupling effects are large and where a critical test of the existing B-phase theories is possible. A complication arises for $P > P_{PCP}$ and for T near T_c because here the strong-coupling effects stabilize the A phase and prevent the B-phase data from extending to T_c. However, a reasonable extrapolation of the data can be made which is thermodynamically consistent. Note first that T_c is not expected to be altered by the existence of the A phase.[38] It then follows quite directly that

$$\frac{L_{A\text{-}B}}{T_{A\text{-}B}} = S_A(T_{A\text{-}B}) - S_B(T_{A\text{-}B}) = \int_{T_{A\text{-}B}}^{T_c} \frac{C_B - C_A}{T} dt \ , \quad (19)$$

which is the constraint under which the extrapolations were made. It was assumed that the reduced B-phase specific heat, as plotted in Fig. 18, was linear between $T_{A\text{-}B}$ and T_c. The resulting values of $\Delta C/C_> \mid_B$ are given in Figs. 18(g)–18(i).

Figure 19 shows $\Delta C/C_>$ for both the A and B phases plotted against the inverse of the molar volume. To within the precision of the data, the specific-heat jump is proportional to the density. Again, the jump closely approaches the weak-coupling value as the sample pressure is reduced to zero. For pressure greater than P_{PCP} thermodynamics requires the A-phase jump to be larger than the B-phase values. However, in the weak-coupling limit, the A-phase jump is smaller by a factor of $\frac{5}{6}$.[38] The experimental $\Delta C/C_>$ results are insensitive to errors in the temperature scale or in the energy measurements. They do depend, though, on the discontinuous correction applied to account for the amount of sample which remains normal below T_c (Sec. III B). This correction increases the size of $\Delta C/C_>$. At $P=0$ the correction is largest and is $\sim 4\%$.

Comparison with previous determinations of the B-phase specific-heat jump is made in Fig. 20, where the independent variable is now pressure. The agreement is within the combined experimental uncertainties although the earlier results do fall systematically below the new values by several percent. A portion of the discrepancy between the values of Haavasoja and co-workers and our own can be attributed to the smaller correction applied by Haavasoja and co-workers for the normal liquid layer on the sintered-silver heat exchanger (Sec. III B). For $P \lesssim 10$ bars the comparison is further complicated by the anomalous contribution to the normal-phase specific heat which the data of Haavasoja and co-workers exhibited. The squares with no asterisk plotted in Fig. 20 are the values of Haavasoja and co-workers for $\Delta C/C_>$ computed with $C_> = \gamma R T_c + C_{excess}$. The squares *with* the aster-

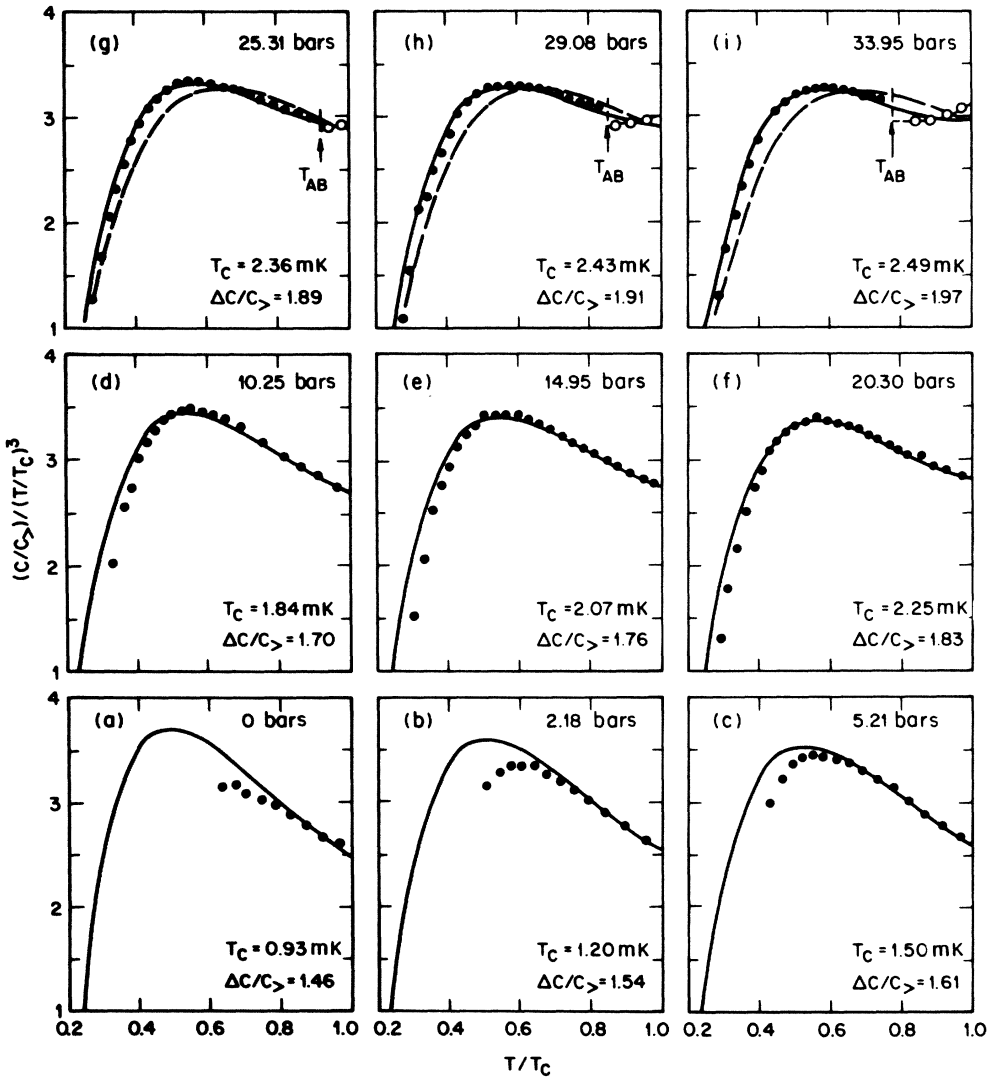

FIG. 18. Reduced plots of the superfluid specific heat measured at nine different sample pressures. The solid curves are the WCP theory of Serene and Rainer (Ref. 13); the long-dashed curves are the phenomenological theory of Padamsee *et al.* (Ref. 41). Both sets of theory curves have been normalized to give the experimental specific-heat jump at T_c.

isks are the specific-heat jumps computed using $C_> = \gamma R T_c$. Since neither our specific-heat data nor the data of Zeise *et al.* show evidence of this excess contribution, it cannot be associated with the bulk liquid. Thus the second analysis should give the more correct results. The fact that the values with asterisks pass through an unexpected minimum near 2 bars led Haavasoja and coworkers to favor the first set of values.

The results of Zeise *et al.*[2] are shown as open triangles in Fig. 20 and are seen to nearly coincide with the results of Ref. 1. We note that in the experiment of Ref. 2, performed using a torsional oscillator, no silver sinter was needed in their calorimeter, and therefore no corrections had to be made for surface effects. However, they did observe a background contribution which they associated with magnetic impurities in their copper heater wire. At low pressure their data exhibit an anomaly in the *superfluid* phase; C/T^3 (refer to Fig. 18) shows an upward curvature near T_c and reaches T_c with a positive slope. The analysis of Ref. 2 favored their lowest-temperature data. The triangles with the asterisk correspond to a simple extrapolation of the data to T_c. We also note that at 29 bars their data are not sufficiently precise to show the discontinuity at $T_{A\text{-}B}$. From this we conclude that the error bars on their higher-pressure data are also large enough to include our values.

The open circle shows the result of Halperin *et al.*[3] obtained at melting pressure. Other earlier results[39,40] are of lesser precision and are not shown in the figure. These values also fall below our values.

The dashed curves shown in Fig. 18 correspond to the phenomenological theory of Padamsee *et al.*[41] In this theory, which applies only for the B phase, the energy gap is related to the weak-coupling gap by a constant scaling factor. Applying this factor f leaves the entropy at T_c unchanged but increases the specific-heat jump by a factor

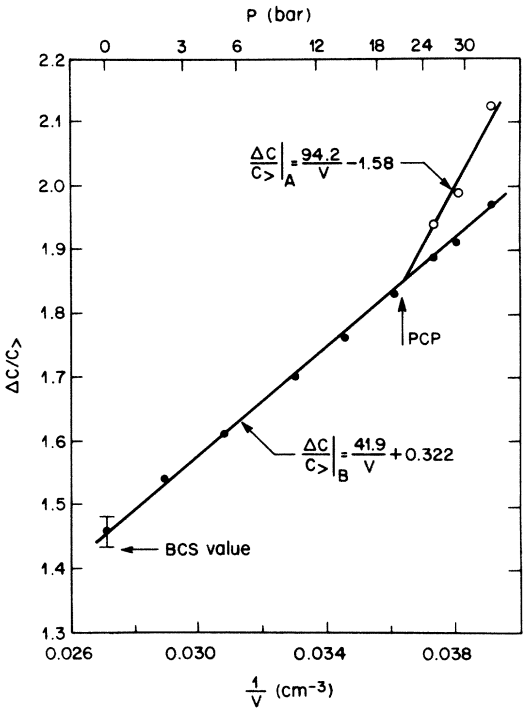

FIG. 19. Specific-heat jump at T_c as a function of the sample density. The solid and open circles refer to the B and A phases, respectively.

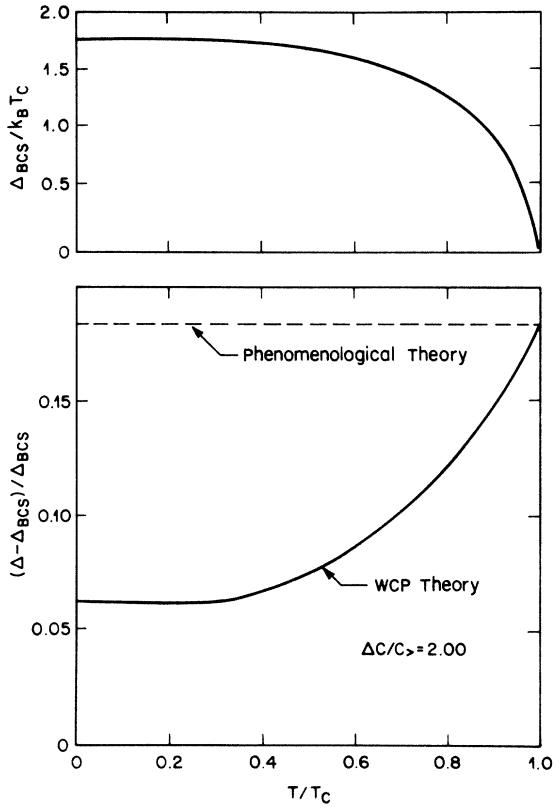

FIG. 21. Comparison of the energy gaps from the WCP (Ref. 13) model and from the scaled BCS theory (Ref. 41).

of f^2. With both S and C at T_c fixed at the experimental values, the temperature dependence of the specific heat below T_c is guaranteed to be at least qualitatively correct.

The solid curves in Fig. 18 were computed using the weak-coupling-plus (WCP) theory of Serene and Rainer[42] as modified by Sauls and Serene.[43] In this quasiclassical theory the strong-coupling corrections to the free energy of superfluid ^{3}He are expressed in terms of the normal-state scattering amplitudes for quasiparticles interacting on the Fermi surface. Because the scattering amplitudes are not known sufficiently accurately the specific-heat jump at T_c becomes the single adjustable parameter. Figure 21 shows the temperature dependence of the gap computed for $\Delta C/C_> = 2$ plotted relative to the corresponding BCS values. Comparison is made with the scaled BCS theory.[41]

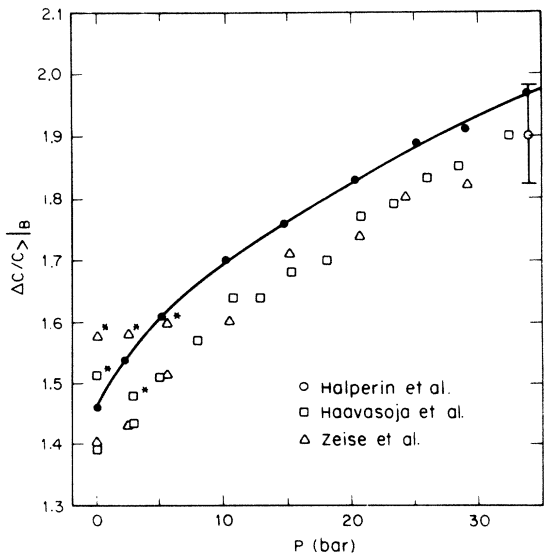

FIG. 20. Comparison of $\Delta C/C_>$ obtained for the B phase from various specific-heat experiments.

Clearly, the WCP theory provides the better overall description of the experimental data, Fig. 18. There are, however, deviations which may be significant. At the three highest pressures and for temperatures near T_c the WCP curves fall systematically below the experimental data. The discrepancy is small and may be due to experimental difficulties, but we note that the higher-pressure data of Haavasoja and co-workers[1] show a similar tendency. The disagreement cannot be removed by using a larger value of $\Delta C/C_>$ since the WCP curves for various values of $\Delta C/C_>$ pass through a common point near $T/T_c = 0.8$. The departures from the theory may therefore be an indication that other strong-coupling effects are significant.

IV. SUMMARY

The specific heat of pure liquid ^{3}He was precisely measured at several sample pressures and at temperatures extending to below 1 mK using the standard heat-pulse technique. The calorimeter was constructed mainly of

silver and had a 10-m^2 sintered-silver heat exchanger in the lower portion of the 17-cm^3 sample chamber. Also located inside the cell were a 116-Ω heater and a LCMN thermometer. Thermal connection between the calorimeter and the nuclear demagnetization refrigeration was via a superconducting heat switch. The parasitic heat leak into the calorimeter was approximately 0.1 nW.

The LCMN thermometer was calibrated using susceptibility bridge readings at T_A, $T_c(0)$, and T_W. Because of the uncertainties in T_A and $T_c(0)$, several different calibrations were performed based on various choices for these transition temperatures. T_W was fixed at the NBS value, 15.57 mK. Using currently accepted values for T_A and $T_c(0)$ led to a low-temperature normal-phase specific heat which was not linear in T and which therefore contradicted previous specific-heat results and also the Landau theory. There were no indications that the discrepancy was due to experimental difficulties. Therefore the departures from linearity were treated as evidence that the commonly used very-low-temperature scales are seriously in error.

A new temperature scale was determined by adjusting T_A and $T_c(0)$ to yield a linear, $P=0$, normal-phase specific heat with a slope in agreement with that extracted from higher-temperature specific-heat measurements. Input to the new scale was also derived from an analysis of the addendum contribution to the total heat capacity. On the new scale $T_A/T_c(0)=2.68$, in excellent agreement with recent Pt NMR results; however, $T_A=2.49$ mK, which is substantially smaller then might have been expected. Using the ^{3}He phase diagram as a comparison standard, it was shown that the scale of Ref. 1 differs from the new scale by a factor of 0.89. The difference between the magnetic temperature scale of Ref. 31 and the proposed thermodynamic scale is uniformly 0.13 mK.

A reanalysis of the measurements of Ref. 1 based on the new temperature scale increased their specific heat by ~20% and brought them into good agreement with the present results. The very large discrepancies between the various sets of normal-phase specific-heat data can thus be explained as being due almost entirely to thermometry errors. The problem then shifts to reconciling the new temperature scale with the older scales. Evidence was presented which showed that the uncertainties in the older scales are much larger than reported and thus that $T_A=2.49$ mK cannot be rigorously excluded by previous work.

The new low-temperature normal-phase specific-heat results are at all pressures proportional to T and show no evidence of the excess contribution observed in Ref. 1 and attributed to an intrinsic property of bulk liquid ^{3}He. Consequently, the size of the specific-heat jumps at T_c could be determined with greater certainty. At $P=0$, $\Delta C/C_>=1.46$, which is very close to the BCS value, 1.43. $\Delta C/C_>$ was found to be proportional to sample density and reaches a value of about 2.0 at the melting curve. Although the new results for $\Delta C/C_>$ versus P are systematically larger than the earlier determinations, agreement is within the combined experimental uncertainties.

The temperature dependence of the specific heat in the B phase is in reasonably good agreement with the WCP

TABLE VII. ^{3}He-melting-curve coordinates determined using Eq. (A1).

T (mK)	$P-P_A$ (bars)	dP/dT (bars K^{-1})	T (mK)	$P-P_A$ (bars)	dP/dT (bars K^{-1})	T (mK)	$P-P_A$ (bars)	dP/dT (bars K^{-1})
0.931 (T_c)	0.052 52	−27.2	4.0	−0.057 52	−39.2	80.0	−2.566 06	−25.1
1.0	0.050 55	−29.2	5.0	−0.097 12	−39.9	85.0	−2.689 17	−24.2
1.1	0.047 54	−30.8	6.0	−0.137 20	−40.2	90.0	−2.807 83	−23.3
1.2	0.044 41	−31.7	7.0	−0.177 50	−40.3	95.0	−2.922 15	−22.4
1.3	0.041 21	−32.2	8.0	−0.217 86	−40.3	100.0	−3.032 29	−21.6
1.4	0.037 97	−32.7	9.0	−0.258 18	−40.3	110.0	−3.240 51	−20.0
1.5	0.034 68	−33.1	10.0	−0.298 39	−40.2	120.0	−3.433 50	−18.6
1.6	0.031 35	−33.5	11.0	−0.338 47	−40.0	130.0	−3.612 23	−17.2
1.7	0.027 98	−33.9	12.0	−0.378 37	−39.8	140.0	−3.777 57	−15.9
1.8	0.024 56	−34.3	14.0	−0.457 61	−39.4	150.0	−3.930 35	−14.7
1.9	0.021 11	−34.7	16.0	−0.536 00	−39.0	160.0	−4.071 28	−13.5
1.932 ($T_{A\text{-}B}$)	0.020 00	−34.8	18.0	−0.613 50	−38.5	170.0	−4.200 97	−12.4
2.0	0.017 63	−35.1	20.0	−0.690 07	−38.0	180.0	−4.319 95	−11.4
2.1	0.014 10	−35.4	25.0	−0.877 34	−36.9	190.0	−4.428 59	−10.4
2.2	0.010 55	−35.7	30.0	−1.058 66	−35.7	200.0	−4.527 14	−9.4
2.3	0.006 96	−36.1	35.0	−1.234 06	−34.5	210.0	−4.615 74	−8.4
2.4	0.003 33	−36.4	40.0	−1.403 63	−33.3	220.0	−4.694 32	−7.4
2.491 (T_A)	0.000 00	−36.6	45.0	−1.567 50	−32.2	230.0	−4.762 70	−6.3
2.5	−0.000 32	−36.6	50.0	−1.725 79	−31.1	240.0	−4.820 50	−5.2
2.6	−0.003 99	−36.9	55.0	−1.878 63	−30.0	250.0	−4.867 17	−4.1
2.7	−0.007 69	−37.1	60.0	−2.026 16	−29.0			
2.8	−0.011 42	−37.4	65.0	−2.168 53	−28.0			
2.9	−0.015 17	−37.6	70.0	−2.305 88	−27.0			
3.0	−0.018 94	−37.8	75.0	−2.438 34	−26.0			

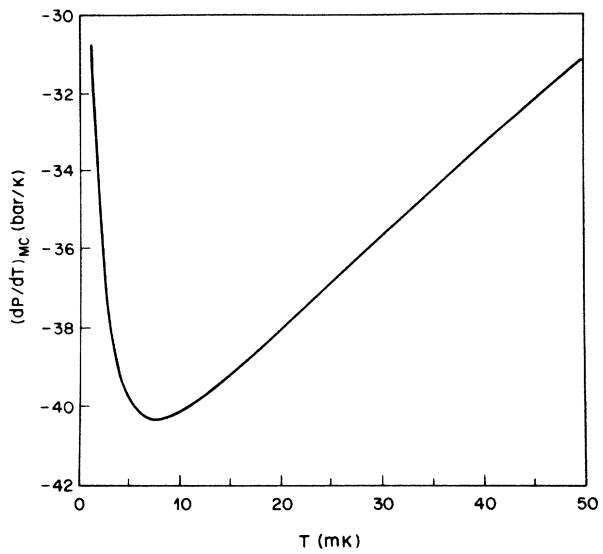

FIG. 22. Slope of the ^{3}He melting curve described by Eq. (A1).

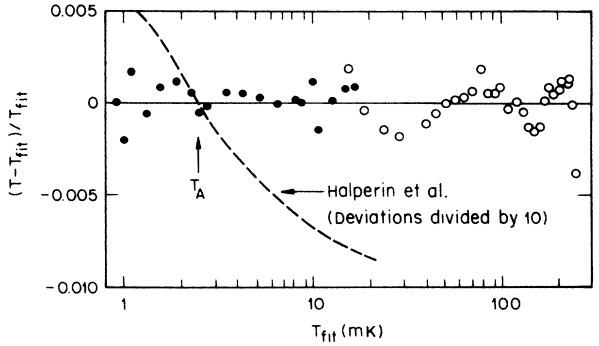

FIG. 23. ^{3}He-melting-curve data plotted as deviations from Eq. (A1). The solid circles are new data; the open circles are the results of Greywall and Busch (Ref. 24) corrected to account for revisions in the NBS temperature scale.

theory of Serene and Rainer; however, discrepancies are observed at high pressure and near T_c.

ACKNOWLEDGMENTS

I am very grateful to J. A. Sauls for supplying the computer program for the WCP B-phase specific heat and to P. A. Busch for his technical assistance.

APPENDIX: ^{3}He MELTING-CURVE CALIBRATION

The LCMN thermometer calibration used to obtain the specific-heat data presented in this paper has also been used to determine the P-T coordinates for ^{3}He along the melting curve for $T \lesssim 15$ mK. These new data and also previous higher-temperature data are described well by the relation

$$P - P_A = \sum_{n=-3}^{5} a_n T^n , \tag{A1}$$

with

$a_{-3} = -0.196\,529\,70 \times 10^{-1}$, $a_{-2} = 0.618\,802\,68 \times 10^{-1}$,

$a_{-1} = -0.788\,030\,55 \times 10^{-1}$, $a_0 = 0.130\,506\,00$,

$a_1 = -0.435\,193\,81 \times 10^{-1}$, $a_2 = 0.137\,527\,91 \times 10^{-3}$,

$a_3 = -0.171\,804\,36 \times 10^{-6}$, $a_4 = -0.220\,939\,06 \times 10^{-9}$,

$a_5 = 0.854\,502\,45 \times 10^{-12}$.

The pressure and temperature are measured in bars and millikelvin, respectively.

A list of smoothed pressure-temperature values is given in Table VII, and the slope of the melting curve is plotted in Fig. 22. Deviations from the fit are shown in Fig. 23 for temperatures less than 250 mK. The solid circles are the present work; the open circles are data from Greywall and Busch[24] corrected[14] to account for recent revisions in the NBS temperature scale.[12] The dashed curve shows the results of Halperin *et al.*[3] assuming $T_A = 2.491$ mK.

Over the last several years we have presented several different MC calibrations; the differences are briefly summarized in the following:

Calibration A (1982) (Ref. 24): Temperatures in this work were measured using a LCMN (10 at.% CMN) thermometer for $7 \lesssim T \lesssim 15$ mK and a pure-CMN thermometer for $15 \lesssim T \lesssim 330$ mK. These thermometers were calibrated using the NBS fixed points at 100, 160, and 200 mK and the condition that the implied P-T coordinates of the MC agree with the data of Halperin *et al.* ($T_A = 2.752$) for $7 \lesssim T \lesssim 20$ mK. The tacit assumption was made that the Δ's for both thermometers were the same, namely 0.7 mK. The two pressure scales were normalized to agree at the minimum in the melting curve, $P_{\min}$. On this scale $T_W = 15.93$ mK.

Calibration B (1983) (Ref. 8): This calibration is based on the same measurements used for calibration A, but here Δ was determined by the condition that the specific heat of normal ^{3}He be linear in T for temperatures extending down to 7 mK. This method of calibration led to a CMN Δ of 0.40 mK and to $T_W = 15.74$ mK. The splice to the data of Halperin *et al.* was made by uniformly shifting the pressure coordinates of their data by 10 mbar. Pressures were again measured relative to $P_{\min}$.

Calibration C (1985) (Ref. 14): This calibration is again based on the same measurements as calibrations A and B. However, the CMN thermometer was now calibrated using the revised NBS (CTS-1983) temperatures for the fixed points at 100, 160, 200 mK and also for the tungsten sample at 15.57 mK. The CMN Δ was now found to be 0.29 mK. $T_{\min} = 0.316$ K. The data of Halperin *et al.* were forced to agree with the higher-temperature results at 15 mK by assuming $T_A = 2.71$ mK. Pressures were now measured relative to P_A.

Calibration D: This is the MC calibration presented in this paper. It is based on the same high-temperature (i.e., $T > 15$ mK) P-T data as calibration C, but on new data obtained with a LCMN thermometer at lower temperatures. Details of the LCMN-thermometer calibration are given in the body of this paper. Pressures are measured relative to P_A.

[1]T. Haavasoja, Ph.D. thesis, Helsinki University of Technology, 1980 (unpublished); T. A. Alvesalo, T. Haavasoja, and M. T. Manninen, J. Low Temp. Phys. **45**, 373 (1981); T. A. Alvesalo, T. Haavasoja, M. T. Manninen, and A. T. Soinne, Phys. Rev. Lett. **44**, 1076 (1980).

[2]E. K. Zeise, Ph.D. thesis, Cornell University, 1981 (unpublished); E. K. Zeise, J. Saunders, A. I. Ahonen, C. N. Archie, and R. C. Richardson, Physica (Utrecht) **108B**, 1213 (1981).

[3]W. P. Halperin, F. B. Rasmussen, C. N. Archie, and R. C. Richardson, J. Low Temp. Phys. **31**, 617 (1978).

[4]A. C. Anderson, W. Reese, and J. C. Wheatley, Phys. Rev. **130**, 495 (1963).

[5]W. R. Abel, A. C. Anderson, W. C. Black, and J. C. Wheatley, Phys. Rev. **147**, 111 (1966).

[6]A. C. Mota, R. P. Platzeck, R. Rapp, and J. C. Wheatley, Phys. Rev. **177**, 266 (1969).

[7]B. Hebral, G. Frossati, H. Godfrin, and D. Thoulouse, Phys. Lett. **85A**, 290 (1981).

[8]D. S. Greywall, Phys. Rev. B **27**, 2747 (1983).

[9]M. C. Mayberry, W. E. Fogle, and N. E. Phillips, in *Quantum Fluids and Solids,* edited by E. D. Adams and G. G. Ihas (AIP, New York, 1983), p. 161.

[10]B. Sen and C. N. Archie, Phys. Rev. B **29**, 1490 (1984).

[11]K. Levin and O. T. Valls, Phys. Rep. **98**, 1 (1983).

[12]J. H. Colwell, W. E. Fogle, and R. J. Soulen, Jr., in *Proceedings of the 17th International Conference on Low Temperature Physics,* edited by U. Eckern, A. Schmid, W. Weber, and H. Wühl (North-Holland, Amsterdam, 1984), Pt. 1, p. 395; and private communication.

[13]J. W. Serene and D. Rainer, Phys. Rep. **101**, 221 (1983).

[14]D. S. Greywall, Phys. Rev. B **31**, 2675 (1985).

[15]72 at. % silver, 28 at. % copper. The soldering was done in an oven, under a ^{4}He atmosphere and as quickly as possible.

[16]Vacuum Metallurgical Co., Tokyo, Japan, 400-Å powder.

[17]400 °C, 15 min, ^{4}He atmosphere.

[18]Emerson and Cuming, Canton, MA, type 1266.

[19]P. A. Busch, S. P. Cheston, and D. S. Greywall, Cryogenics **24**, 445 (1984).

[20]Materials Research Corporation, Orangeburg, NY.

[21]Emerson and Cuming, Canton, MA, type 2850FT.

[22]W. O. Sprenger (unpublished).

[23]E. I. Dupont de Nemours, Polymer Products Department, Wilmington, DE, type SP-22.

[24]D. S. Greywall and P. A. Busch, J. Low Temp. Phys. **46**, 451 (1982).

[25]P. R. Roach, J. B. Ketterson, and Kuchmir, Rev. Sci. Instrum. **43**, 898 (1972).

[26]D. S. Greywall, Phys. Rev. B **18**, 2127 (1978).

[27]J. C. Wheatley, Rev. Mod. Phys. **47**, 415 (1975).

[28]R. B. Kummer, R. M. Mueller, and E. D. Adams, J. Low Temp. Phys. **27**, 319 (1977).

[29]D. D. Osheroff and C. Yu, Phys. Lett. **77A**, 458 (1980).

[30]D. D. Osheroff (private communication).

[31]D. N. Paulson, M. Krusius, J. C. Wheatley, R. S. Safrata, M. Kolăc, T. Těthal, K. Svec, and J. Matas, J. Low Temp. Phys. **34**, 63 (1979); **36**, 721(E) (1979).

[32]O. Avenel, M. Bernier, D. Bloyet, P. Piejus, E. Varaquaux, and C. Vibet, in *Proceedings of LT-14 (Otaniemi, Finland),* edited by M. Krusius and M. Vuorio (North-Holland, Amsterdam, 1975), Vol. 4, p. 64.

[33]A. I. Ahonen, M. Krusius, and P. A. Paalanen, J. Low Temp. Phys. **25**, 421 (1976).

[34]A. I. Ahonen, M. T. Haikala, M. Krusius, and O. V. Lounasmaa, Phys. Rev. Lett. **33**, 628 (1974).

[35]D. N. Paulson, M. Krusius, and J. C. Wheatley, J. Low Temp. Phys. **25**, 699 (1976).

[36]R. C. Richardson, Physica **90B**, 47 (1977).

[37]E. Lhota, M. T. Manninen, J. P. Pekola, A. T. Soinne, and R. J. Soulen, Phys. Rev. Lett. **47**, 590 (1981).

[38]A. J. Leggett, Rev. Mod. Phys. **47**, 331 (1975).

[39]R. A. Webb, T. J. Greytak, R. T. Johnson, and J. C. Wheatley, Phys. Rev. Lett. **30**, 210 (1973).

[40]K. Andres and S. Darack, Physica (Utrecht) **86-88B**, 1071 (1977).

[41]H. Padamsee, J. E. Neighbor, and C. A. Shiffman, J. Low Temp. Phys. **12**, 387 (1973).

[42]J. W. Serene and D. Rainer, J. Low Temp. Phys. **34**, 589 (1979).

[43]J. A. Sauls and J. W. Serene, Physica **108B**, 1137 (1981).